Estimating GATE Rainfall with Geosynchronous Satellite Images

JOHN E. STOUT AND DAVID W. MARTIN

Space Science and Engineering Center, Madison, WI 53706

DHIRENDRA N. SIKDAR

University of Wisconsin, Milwaukee, WI 53201

(Manuscript received 6 November 1978, in final form 7 February 1979)

ABSTRACT

A method of estimating GATE rainfall from either visible or infrared images of geosynchronous satellites is described. Rain is estimated from cumulonimbus cloud area by the equation $R = a_0A + a_1dA/dt$, where R is volumetric rainfall ($m^3 s^{-1}$), A cloud area (m^2), t time (s), and a_0 and a_1 are constants. Rainfall, calculated from 5.3 cm ship radar, and cloud area are measured from clouds in the tropical North Atlantic. The constants a_0 and a_1 are fit to these measurements by the least-squares method. Hourly estimates by the infrared version of this technique correlate well (correlation coefficient of 0.84) with rain totals derived from composited radar for an area of 10^5 km^2. The accuracy of this method is described and compared to that of another technique using geosynchronous satellite images. We conclude that this technique provides useful estimates of tropical oceanic rainfall on a convective scale.

1. Introduction

To adequately describe convective rainfall, meteorologists have supplemented the point measurements of gages with area measurements of radar. Calibrated radar provides excellent information over a 200 km range. For larger areas and over the oceans, satellites may be needed. Thus in the design of the Global Atmospheric Research Program Atlantic Tropical Experiment (GATE), coverage of rainfall on synoptic and larger scales was to be provided by two satellites: Nimbus 5, with a microwave sensor, and the first Synchronous Meteorological Satellite, with visible and infrared sensors (Houghton, 1974).

The Nimbus microwave instruments directly measure rainfall (Wilheit *et al.* 1977), but their sampling interval and spacial resolution are large compared to the lifetime and scale of most convective disturbances. Although visible and infrared sensors do not respond directly to hydrometeors, the high temporal and spacial resolution of geosynchronous satellite observations is a singular advantage in indirect measurements of convective rainfall (Martin and Scherer, 1973).

Scofield and Oliver (1977) describe a technique to estimate station (point) rainfall in the central United States using infrared and visible hard copy images of a geosynchronous satellite. They include as determinants of rainfall cloud-top temperature, rate of anvil growth, position within the anvil, mergers of cells and lines, and overshooting tops. Rainfall rate is assigned through a series of binary or trinary decisions.

A technique based on area measurements from infrared or visible digital images of a geosynchronous satellite is described by Griffith *et al.* (1978). Volumetric rain rate is estimated from convective cloud area through a time-dependent empirical relation between cloud area, echo area and volumetric rain rate. The present paper describes a variant of this technique, in which volumetric rain rate is related directly to cloud area and area change, using a meteorologist to determine and measure convective cloud area. This so-called University of Wisconsin (UW) scheme is aimed at providing convective rain estimates on scales comparable with those of radar. Its assumptions follow:

- *Almost all tropical precipitation comes from organized deep convection.* Riehl and Malkus (1958) concluded that synoptic-scale disturbances and cumulonimbus towers within them accomplish most of the vertical energy transport in the equatorial tropics. Evidence is presented in the Appendix that the overwhelming bulk of rainfall in the tropical east Atlantic comes from cumulonimbus clouds.
- *Cumulonimbi can be readily identified in synchronous satellite images.* Brightness (in visible images) or coldness (in infrared images) and expansion are the primary criteria for distinguishing

0027-0644/79/050585-14$07.50

cumulonimbus clouds. The cloud's shape and motion relative to small cumulus and cirrus are also useful.

• *Cumulonimbus cloud area and area change are related to rainfall.* Cloud area, defined as area within a threshold contour of brightness or temperature, will relate to rainfall if the threshold has skill in discriminating between parts of the satellite image more likely or less likely to contain rain. The existence of significant skill, beyond the obvious condition that rain only occurs in association with clouds, is indicated by many studies relating visible satellite brightness to rainfall (Martin and Suomi, 1972; Woodley and Sancho, 1971; Kilonsky and Ramage, 1976). Window infrared sensors see the heights of the tops of most clouds. If a cloud is also deep, as we select them to be, the infrared radiance threshold will discriminate between raining and non-raining cloud. Change of cloud area has been shown to be related to rainfall by Sikdar (1972).

We combine cumulonimbus cloud area and its change in a simple rain estimating equation:

$$R = a_0 A + a_1 dA/dt, \quad (1)$$

where R is the volumetric rainfall of the cloud (m^3 s^{-1}), A the cloud area (m^2), dA/dt the change of cloud area over time (m^2 s^{-1}), and a_0 and a_1 are constants with dimensions meters per second and meters, respectively. In the sections below we describe the approach and data used to establish the coefficients a_0 and a_1, give the relationships found between cloud area and volumetric rain rate, present the results of a test for the GATE area, and evaluate the accuracy of the technique. Results from the present technique are then compared with rainfall estimated from another version of the technique described by Griffith *et al.* (1978).

2. Measuring techniques and data

a. General procedure

Our data processing begins by defining the area of a cloud. We select a threshold value of brightness (for visible images) and one of coldness (for infrared images). This value is chosen so that nearly all convective clouds fall within its contour on the satellite image. Next, we measure cloud area[1] on the satellite image and the corresponding volumetric rainfall rate (calculated from echo area measured at several reflectivity levels) on the radar image for a cloud through its life. These measurements are repeated for a number of clouds. Finally, we use these cloud area–rain rate pairs to calculate the constants a_0 and a_1 of Eq. (1) by a least-squares fit.

[1] Henceforth, cloud area will mean the area seen in an infrared or visible satellite image, defined by a threshold value.

b. Measurement of cloud area and rainfall

Matching satellite and radar images are displayed on the University of Wisconsin's image processing system McIDAS (Chatters and Suomi, 1975). A looping capability allows the operator to follow the evolution of the cloud before measuring. He then draws an outline around a cloud and the computer calculates the area inside the outline and higher than the threshold value. When clouds overlap, the looping helps in determining where to divide them. Radar echoes, on an opposing loop, are associated with the corresponding clouds and measured for rain.

c. Data

Visible images with 1 km by 1 km resolution and infrared images with 4 km by 8 km resolution from the first Geosynchronous Meteorological Satellite (SMS 1) are used. These are navigated (Smith and Phillips, 1972) and the visible images are normalized for changing sun-cloud-satellite geometry (Mosher, 1975). Calibrated C-band ship radar data are corrected for platform instability by using the maximum value of the two lowest scans (Hudlow and Patterson, 1979) and corrected for mean bias and atmospheric attenuation (Hudlow and Patterson, 1979). The radar images are remapped to the scale and projection of the satellite. We measure echo area within reflectivity contours spaced 3 dB apart. Rain rate is calculated from these area measurements using $Z = 230\,R^{1.25}$ (Hudlow and Patterson, 1979), where Z is reflectivity (mm^6 m^{-3}) and R is rain rate (mm h^{-1}).

3. Cloud area and rainfall relationships

a. A typical cloud

The life cycle of a typical cloud is shown in Fig. 1. Cloud area, in visible and infrared, and volumetric rain rate are plotted against time. Rain precedes cloud area by about an hour, placing it mostly in the growing phase. Note also that the shapes of the rainfall and cloud area curves are roughly similar. Both of these points support the use of cloud area and area change to estimate rain.

b. Choosing a threshold

Images of clouds near Miami, Florida, from an early satellite, the third Applications Technology Satellite (ATS 3), were used to determine the visible threshold for cloud area. The digital count (60) corresponding to an albedo of 0.45 with the sun overhead was chosen because clouds at least this bright have a 50% probability of having any echoes (Fig. 2). Contour area measured at this level is close to the maximum correlation with rainfall (Fig. 3a). The equivalent digital count in SMS 1 is 172. This was

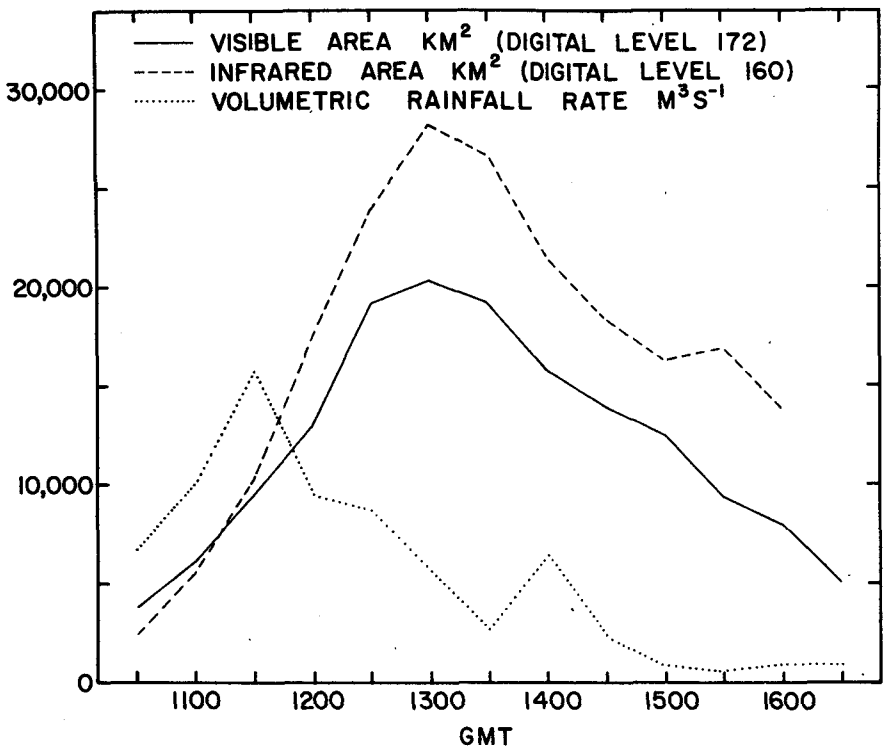

FIG. 1. The evolution of a typical cloud. Cloud area in visible and infrared wavelength images, and volumetric rain rate (measured by radar) are plotted against time.

established by comparing clouds close to Miami viewed by the SMS 1 and ATS 3 (Martin *et al.*, 1975). Area measured at the selected infrared level, 160 digital counts, equivalent to a blackbody temperature of −26°C, is at the correlation maximum in Fig. 3b. Fig. 3 is based on data near the ship *Oceanographer*, located at 22°12′W, 07°45′N. These data were also used to derive the rain estimation

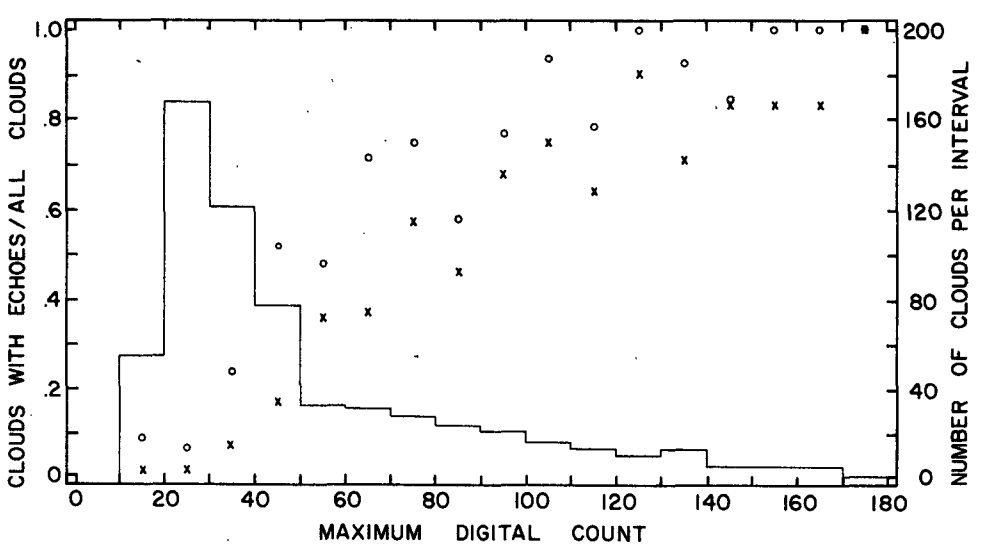

FIG. 2. The number of clouds with echoes (detected by the University of Miami's WSR-57 radar) divided by the total number of clouds plotted against maximum cloud brightness (ATS-3 digital count) for intervals of 10 digital counts. Circles are echo-cloud ratios for all echoes; crosses are echo-cloud ratios for echoes higher than minimum detectable signal. The number of clouds in each interval is shown by the bar graph.

relations in the next section. These thresholds differ by small amounts from the thresholds chosen by Griffith *et al.* (1978). Because the correlation of rainfall and cloud area in this range is insensitive to small changes in threshold value (Fig. 3), for practical purposes the differences are negligible.

c. The rain estimation relations

We followed 23 clouds in visible images occurring on 4 and 6 September 1974, for a total of 219 pairs of cloud area and rainfall measurements (34 clouds and 329 pairs in infrared images). When the constants a_0 and a_1 in Eq. (1) are fit to these data, the rain estimating equations become

$$\text{INFRARED:} \quad R = 5.4 \times 10^{-7}\ (\text{m s}^{-1})\, A + 2.8 \times 10^{-3}\ (\text{m})\, dA/dt, \tag{2}$$

$$\text{VISIBLE:} \quad R = 5.2 \times 10^{-7}\ (\text{m s}^{-1})\, A + 2.6 \times 10^{-3}\ (\text{m})\, dA/dt. \tag{3}$$

d. Discussion of the rain estimation relations

The constants for the infrared and visible equations are quite close, which suggests that the two thresholds, chosen for their ability to separate raining clouds from non-raining clouds, in some sense define a similar area. The relative importance of the area and area change terms is revealed by substituting the mean values of A and $|dA/dt|$ into Eqs. (2) and (3):

$$\text{INFRARED:} \quad R = 3.3 \times 10^{3} + 1.9 \times 10^{3}, \tag{4}$$

$$\text{VISIBLE:} \quad R = 2.3 \times 10^{3} + 1.3 \times 10^{3}. \tag{5}$$

The area term (on the left) is larger than the area change term by a factor of 1.7 in the infrared case and 1.8 in the visible case. Since the integral of dA/dt over the lifetime of the cloud is zero, the area change term can be viewed as compensating for the lag of cloud area behind rainfall shown in Figs. 1 and 3.

The ratio of the standard error of the estimated rainfall over the mean observed (radar) rainfall is 0.76 for the infrared equations and 0.62 for the visible equations. Thus for one cloud for 30 min the expected error (assuming perfect radar measurements of rainfall) is 60–75% of the rain estimate. When estimates are made for areas including several clouds and for longer times this fractional error should decrease. The accuracy of rainfall estimates is discussed further in Section 5.

4. A large-scale test of the method

Thirty-minute rain estimates are made for four cases. Infrared images are used because they are available night and day. The rain estimate for a particular cloud is allocated to a circle centered at the cloud's brightest point, and whose area is equal to one-fifth of the cloud area. The use of one-fifth is a compromise between the average echo area–cloud area ratio of one tenth (Woodley and Sancho, 1971; Martin and Suomi, 1972; Griffith *et al.*, 1976) and spreading the estimate over the entire cloud area.

Hourly rainfall rate is calculated for the GATE master array, a disc 204 km in radius centered at 8°30′N, 23°30′W. These are compared as time series plots (Fig. 4) and as a scatter diagram (Fig. 5) with composited digital radar measurements of rain-

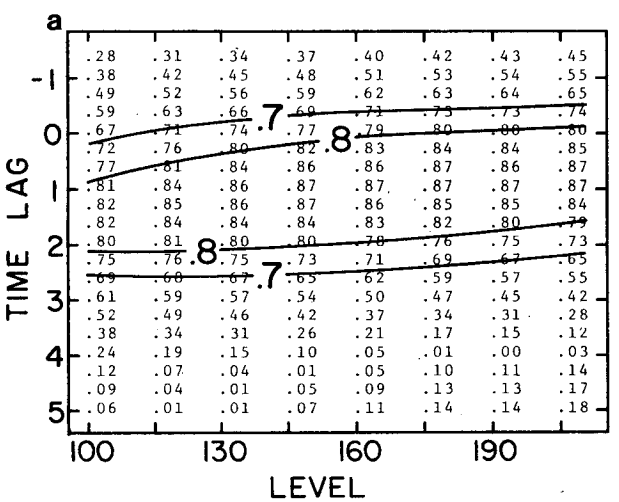

FIG. 3a. Correlations between volumetric rain rate ($m^3 s^{-1}$) and visible cloud area (m^2). Cloud area is measured at threshold levels varying along the abscissa. Correlations are calculated for time lags, indicated in hours along the ordinate.

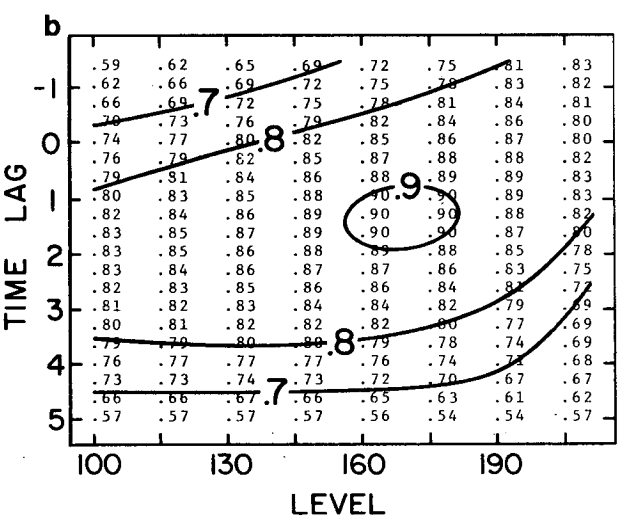

FIG. 3b. As in Fig. 3a but cloud area is measured in the infrared channel.

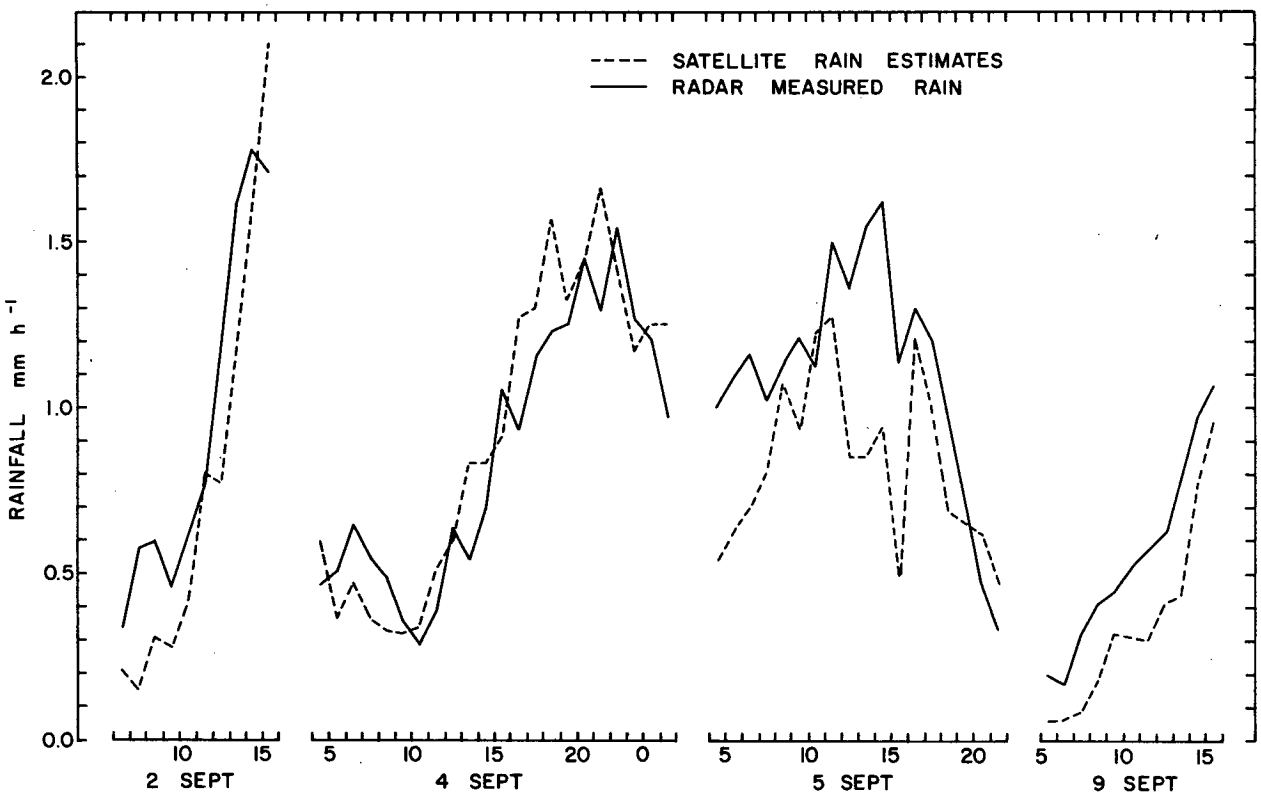

FIG. 4. Hourly satellite estimates of rain falling in the master array compared with radar estimates of rainfall. Hours in GMT are plotted on the abscissa.

fall rate supplied by Hudlow. Calculation of radar rainfall for the master array is described in Hudlow and Patterson (1979). A small overlap exists between the developmental data set and the data used in this test. One-half of the test area is also part of the development area. Data from 4 September, which comprises 65% of the developmental data set, also comprises one-third of the test data set. Thus one-sixth of the test data is part of the data used for development of the cloud area–rainfall relations.

Satellite and radar rainfall agree closely except for three periods: 0700–1000 GMT on 2 September and 0500–0700 and 1200–1600 GMT on 5 September (Fig. 4). In the first two periods, both during morning hours, many small cloud lines were present. Apparently, these lines generate rain without producing as much cirrus as the typical cloud. On the third occasion, the largest cloud occurring that day was present. Because of its size and vigor, this cloud may have been exceptionally efficient in producing rain (Woodley *et al.*, 1971).

The regression of satellite on radar rainfall (Fig. 5) is

$$R_s = -0.05 + 0.91\,R_r\ (\text{mm}), \qquad (6)$$

with a standard error of estimate of 0.25 mm. The correlation coefficient is 0.84 and is significant at the 0.001% level.

5. Accuracy

We wish to state the accuracy, for any scale, of rain estimates made by the present technique. Therefore we examine the error present at various scales (of time and space), defining the error of our estimates as

$$\epsilon = S\bar{R}^{-1}, \qquad (7)$$

where S is the standard deviation of satellite-estimated rainfall minus radar-measured rainfall and $\bar{R}$ the mean radar-measured rainfall. If our sampling is random and the population of errors is normally distributed, ϵ would be simply

$$\epsilon = KN^{-1/2}, \qquad (8)$$

where K is a constant and N the size of our sample (Meyer, 1975).

If Eq. (8) holds, a plot of ϵ vs $N^{-1/2}$ (Fig. 6) would form a straight line intersecting the origin. But such a line extending from point A (the developmental data set) in Fig. 6 passes below point B (the test data set, discussed in the previous section). This can be explained by two additional sources of error not present in point A. First, when estimating for a

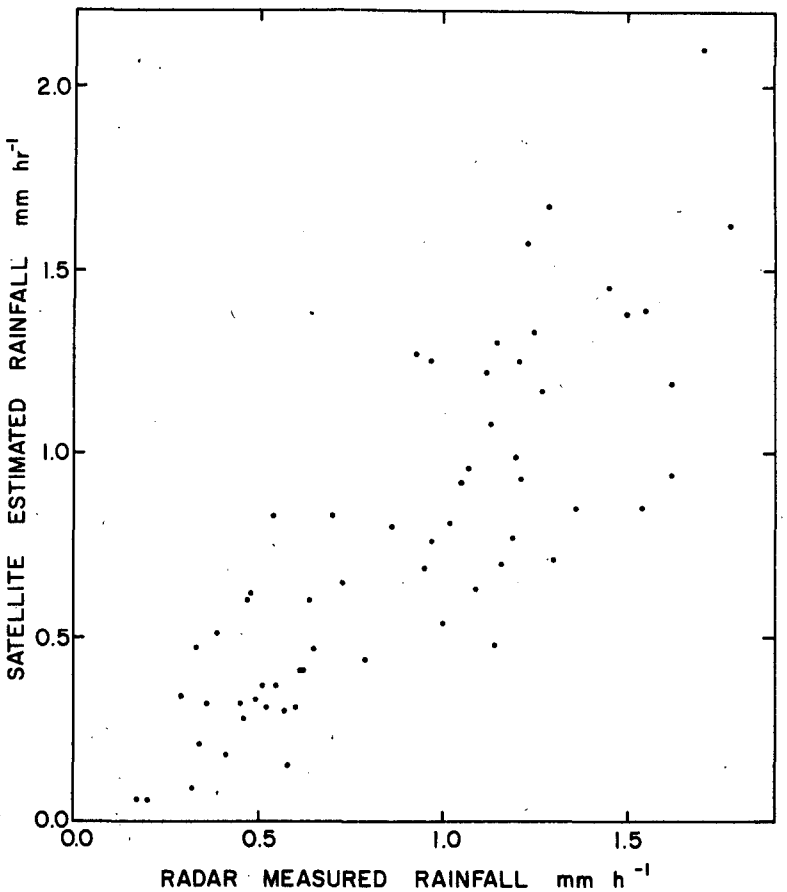

FIG. 5. The data of Fig. 4 plotted as a scatter diagram. Radar estimates are along the abscissa and satellite estimates along the ordinate.

geographical area (point B), the rain estimate is placed around the cloud's brightest point, where the rain may not be. Second, the estimates for point B were done at a coarser scale than those for point A. A straight line extended from point B passes well below point C, yet these points differ only in the length of their time interval: 1 and 6 h, respectively. Certainly there is a strong non-random influence affecting 6 h estimates. Given the prevalence of small cloud lines during morning hours noted in the previous section, it seems likely that this influence is diurnal. There may also be a contribution of sensor sensitivity, discussed below, to a diurnal error.

We may thus construct an error formula for estimates made on a geographical area from Eq. (8) and point B:

$$\epsilon = 7 \times 10^6 (A \times \Delta T \times \mathrm{m^{-2} s^{-1}})^{-1/2}, \qquad (9)$$

where A is the area (m^2) and ΔT is the length of the time interval (s) of the estimate. This formula is valid where ΔT is less than 6 h. If the non-random influence present at a 6 h ΔT is indeed diurnal, then a 24 h estimate should have a low error, perhaps even agreeing with Eq. (9).

Several factors may contribute to the total error. Phase-average radar measurements of rainfall for a single data bin of 16 km^2 are believed (on the basis of radar intercomparisons and comparisons of radar rainfall with ship gage measurements) to be accurate to within 25% (Hudlow and Arkell, 1978). If this error were random and normally distributed, the error in the radar measurement of rainfall for an average satellite cloud of 5000 km^2 and 5 h lifetime would be about 50% (2000 radar observations/bin/phase compared with 600 radar observations/cloud/5 h). However, some of the 25% total error in phase-mean radar rainfall is likely to be due to biases remaining despite all efforts to remove them. The 50% figure therefore is an outside estimate of probable error in the ground truth measurement of total cloud rainfall. The accuracy for any given area and period will depend on the number of cloud estimates included.

Cunning and Sax (1977) offer a Z-R relation different from that used to calculate rainfall in the present study. Their exponent (1.52) gives a rainfall rate 25% smaller at a reflectivity of 40 dBZ, with larger differences at higher reflectivities.

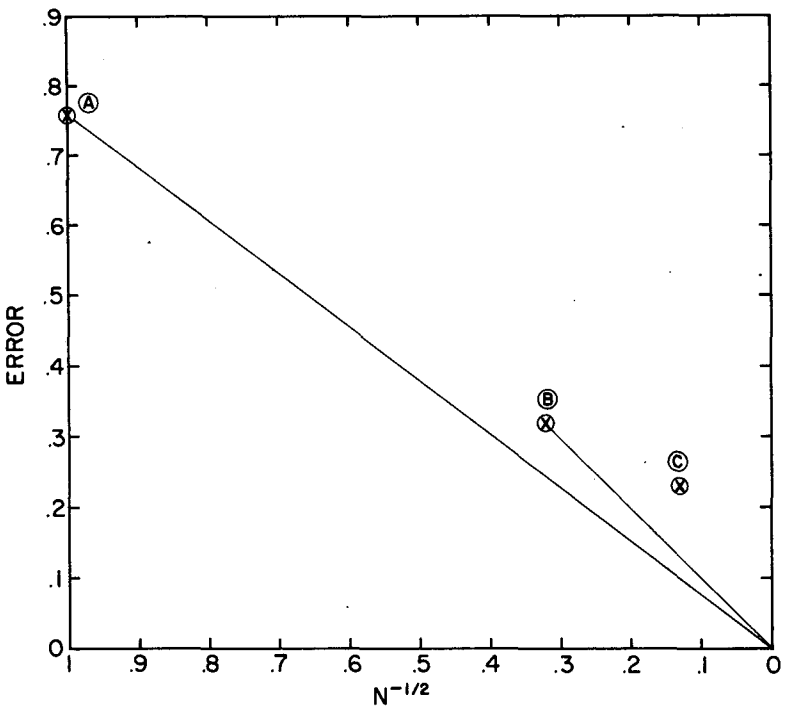

FIG. 6. Error versus sample size (N) for clouds measured in the infrared channel. Error is $\epsilon = S\bar{R}^{-1}$, where S is the standard deviation of satellite estimated rainfall minus radar measured rainfall, and $\bar{R}$ the mean radar measured rainfall. The number of cloud half-hours in an estimate determines the sample size. Point A represents the error of the data set used for development of the rain estimation equation. Point B is the error of the hourly estimates over the master array shown in Fig. 4. Point C uses the same data as Point B, but summed over 6 h intervals.

However, the smaller rainfall rates at high reflectivities tend to be compensated by larger rainfall rates at low reflectivities. If we had used Cunning and Sax's relation, our estimates would be lower by 10%.

A second contribution to error comes in the measurement of cloud area. Over the period of GATE there was a gradual change in the sensitivity of the infrared scanner. Measurements by Lienesch, reported by Smith and Vonder Haar (1976), show that over Phase III (the period of immediate interest), the drift of the infrared sensor at the cloud threshold of 160 digital counts (dc) was about 1.4°C. A drift of this amount produces an error of ±5% in the measurement of cloud area. Considering other sources, this is too small a contribution to total error to warrant correction. [However, departures from the digital count to temperature relation implicit in Eq. (2) were considerably larger earlier in GATE.] A diurnal positive excursion of sensor sensitivity appeared with the onset of satellite eclipse on 24 August (Lienesch, 1974; Bauer and Lienesch, 1975; Smith, 1977). The effect of the increased sensitivity was to decrease the blackbody temperature corresponding to 160 dc by up to 2.5°C, and thus to decrease the area of a threshold cloud measurement. This error is largest just after eclipse, about 0400 to 0600 GMT. Typical errors in area measurement at the peak of the excursion are −10%; thus, though it may be important for individual rain estimates made just after eclipse, this is a minor contributor to total error. Smith (1977) has also noted that the rather slow (55 μs) response time of the infrared sensor produces a smearing as the sensor scans from warm (ocean) to cold (cirrus). This slow response and the fairly coarse resolution of the infrared scanner will combine to underestimate the areas of deep convective clouds. The effect on estimates of rainfall can be significant for small clouds.

Scale imposes a third limitation on satellite estimates of rainfall. The 1:10 average ratio of echo to cloud area is a consequence of looking down on the clouds: the anvil registers more clearly than the cloud towers where precipitation is concentrated (the effect is stronger in infrared than in visible images because of the greater opacity of cloud at longer wavelengths). There are several plausible schemes for allocating rainfall. In all, however, the compromise between accuracy in location of the maximum and accuracy in extent of the rainfall tends to spread the rainfall beyond its actual limits

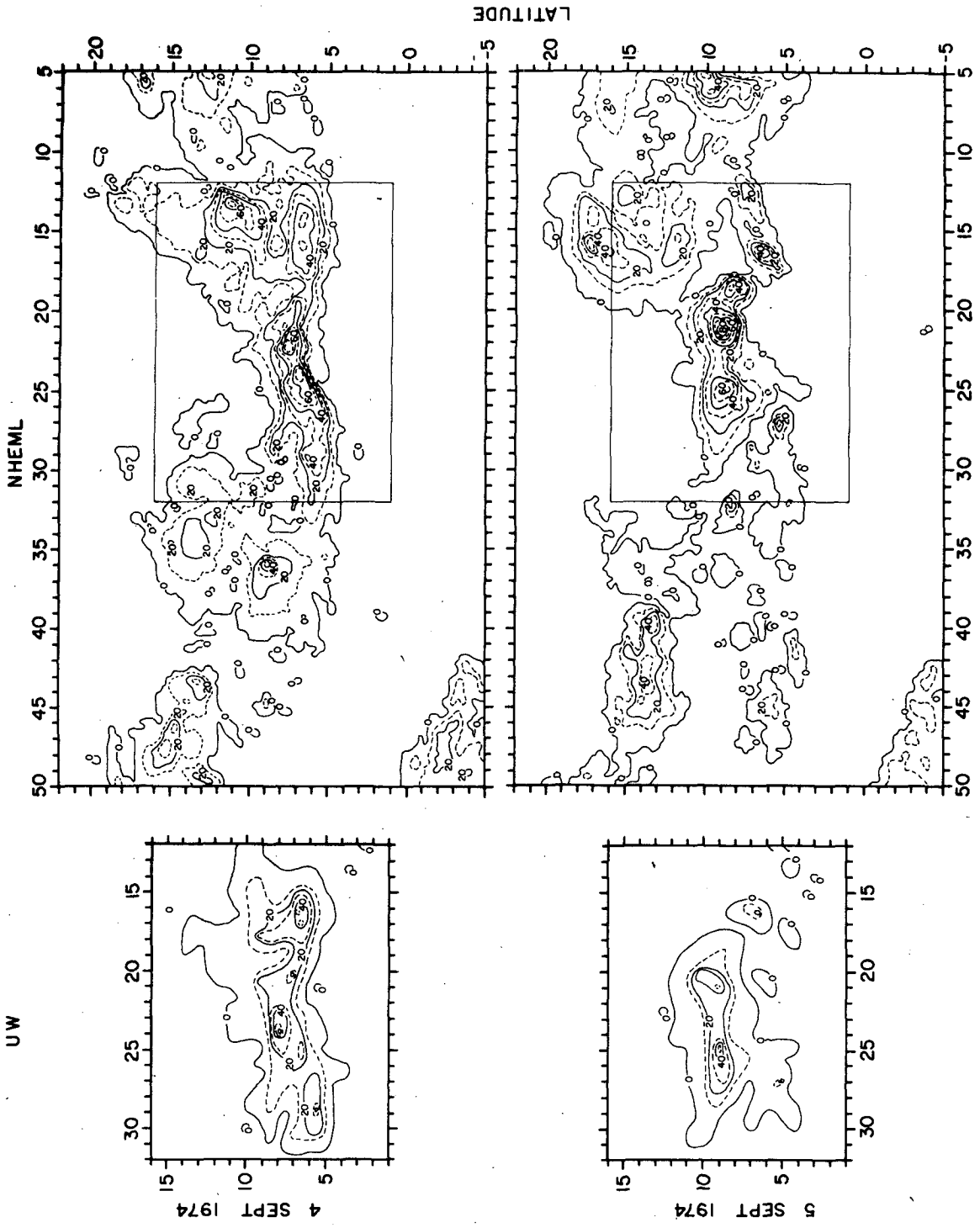

FIG. 7. Comparison of large map products of two satellite rain estimating methods, the one described in this paper (designated UW), and one described by Griffith *et al.* (1978) (designated NHEML). The NHEML maps cover a midnight to midnight GMT time interval. The 4 September UW map covers the period from 0330 GMT on 4 September to 0200 GMT on 5 September, and the 5 September UW map covers the period from 0400 to 2330 GMT on 5 September. The contour interval is 10. Units are millimeters of rain per 24 h. UW coverage is marked as a rectangle on the NHEML map.

for small clouds, but concentrates it for large clouds.

Presently, rainfall is assigned to a circle of area equal to one-fifth of the cloud area centered on the brightest spot within the cloud outline. Where the gradient of brightness across the cloud is flat or where noise is present within the digital data, this point may be distant from the actual location of the highest rainfall. Experience indicates that the separation rarely exceeds a distance equal to the equivalent radius of the cloud.

A fourth contribution to error is our assumption that only deep convective clouds are important to total rain. Shallow convective clouds and non-convective stratiform clouds apparently were not important to total GATE rainfall (see Appendix). They may be of local importance.

The most fundamental limitation on the accuracy of this technique is that it proposes to estimate rainfall, the product of a very complex process, with two predictors, convective cloud area and area change. Because we cannot account directly for each of the many conditions and processes that influence rainfall, we must assume that they are reflected in area and area change, the variables which can be measured. The contribution of this assumption to total error is difficult to reckon. However, this error clearly is minimized if estimates are made only for the area, season and general synoptic conditions of the calibration data.

6. Comparison with another satellite rain-estimation method

Estimates made with the method described in this paper (designated UW) are compared in three ways with estimates made on a synoptic scale by Griffith *et al.* (1979) (designated NHEML), another method using SMS infrared imagery [the technique is that described in Griffith *et al.* (1978) except that the measurement of cloud area and conversion to rainfall have been automated]. Composited C-band shipboard radar (designated CEDDA) provides a standard for comparison.

The first comparison is between large area maps of average daily rainfall for each method (Fig. 7). The NHEML maps cover more area, otherwise the patterns are similar. The second comparison concerns 3° square maps of average daily rainfall (Fig. 8). The pattern of both satellite-generated maps is

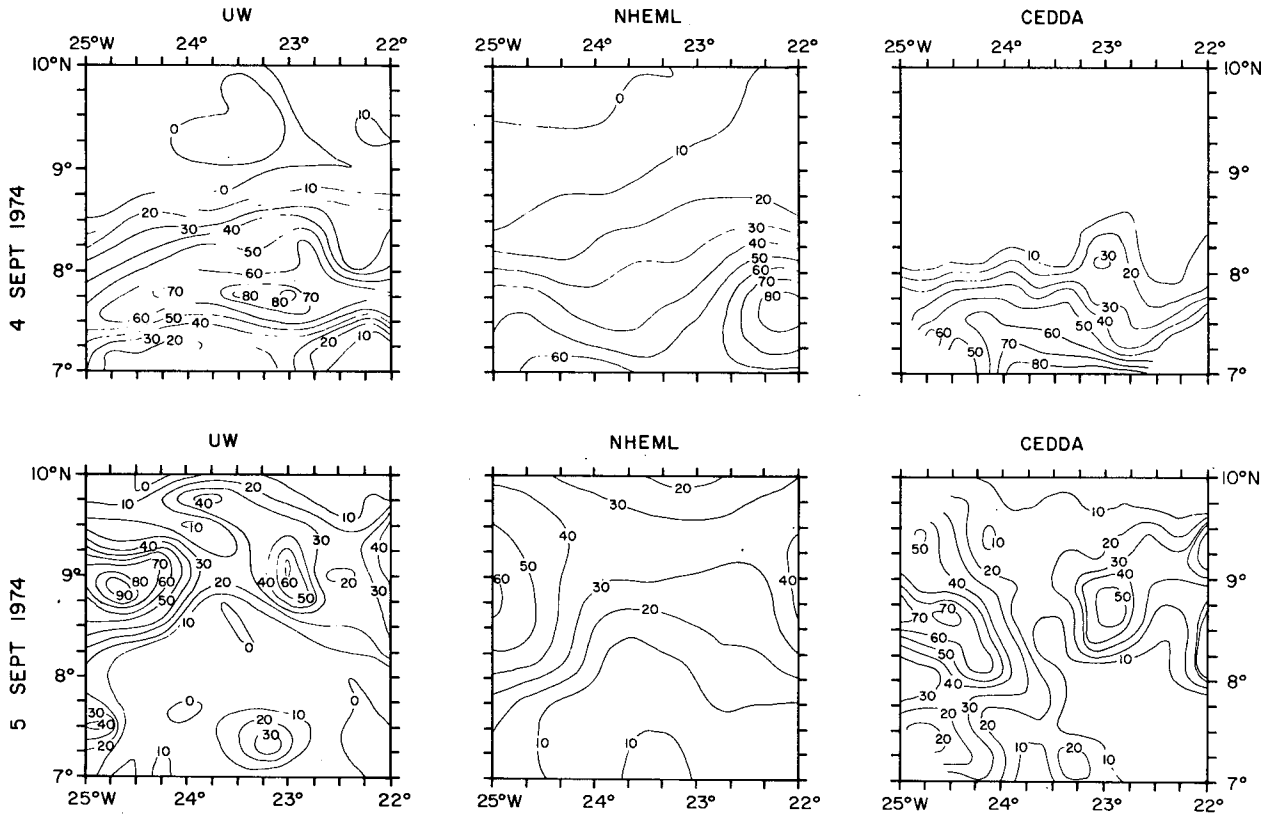

FIG. 8. Comparison of the UW and NHEML satellite, and CEDDA radar methods of estimating rainfall. Contours are drawn every 10 mm of daily rainfall over a 3° square box centered at 8°30′N, 23°30′W. The CEDDA estimates cover a midnight to midnight GMT interval, otherwise the time intervals are as in Fig. 1. Radar rainfall was not calculated in the corners of the CEDDA maps.

shifted north with respect to the radar, probably due to blowing off of cirrus tops. (The shift due to perspective is only 5 km). The UW maps have gradients and numbers of maxima similar to those of CEDDA. The NHEML maps are smoother, probably due to the resolution differences between UW (4 km × 8 km) and NHEML (⅓° × ⅓°). For the third comparison, estimates were totaled for eight 6 h periods over the intersection of a 3° box centered at 8°30'N, 23°30'W and the master array. The root-mean-square difference (satellite minus radar) was 0.16 mm for UW and 0.22 mm for NHEML. The correlation coefficient of UW to CEDDA estimates was 0.87, of NHEML to CEDDA estimates 0.85. The total error was 5% for UW and 12% for NHEML. Some of NHEML's inaccuracy can be traced to their use of Florida data for method development. The data used for the second and third comparisons is the test data set of Section 4, and so suffers from the overlap problem previously discussed.

Both satellite methods compare well to radar. The UW method has an edge in representing detail, though this is achieved at the expense of areal and temporal coverage.

7. Concluding remarks

We conclude that the technique presented in this paper provides useful estimates of convective tropical oceanic rainfall on scales of one hour and tens of kilometers. Given the satellite's ability to follow a disturbance as it moves, this makes the technique a promising tool for cloud cluster convective analysis.

The present technique's main weakness is its inability to handle shallow cloud lines or very large clouds. Treating these as separate cases should improve the estimates. Other refinements likely to improve estimates include taking account of vertical wind shear (Marwitz, 1972) and tropopause height (Scofield and Oliver, 1977), and more realistically distributing rainfall within the cloud.

For use in areas outside the tropical North Atlantic Ocean, the coefficients may need to be rederived. Also, if cumulonimbi are not the major contributors of rain large errors may be made in estimating total rainfall. Another problem could be the presence of large amounts of cirrus. However, this method should work well for vigorous convective systems.

Full accuracy is realized with two consecutive measurements of cloud area. Therefore, where images are immediately available on an interactive display system, such as McIDAS, this technique can provide real-time flood warnings.

Acknowledgments. Special thanks are due Dr. Michael Hudlow of CEDDA for providing radar and rainfall data and helpful advice on their use, and Prof. Geoff Austin of McGill University for providing *Quadra* rainfall data. Dr. Donald Wylie and Mssrs. Brian Auvine and Steven Hentz of the University of Wisconsin helped in outlining clouds. The text was typed by Mrs. Angela Crowell. Figures were drafted by Mr. Tony Wendricks. The support and encouragement of Mr. William Murray of the GATE Project Office, NOAA, has been invaluable. Discussions with colleagues, especially Drs. Donald Wylie, Heinz Lettau and Eberhard Wahl, have been helpful. Finally, we wish to acknowledge the very large contribution of our collaborators from NOAA, Mrs. Cecilia Girz Griffith and Dr. William L. Woodley, and their kind permission to reproduce parts of Figs. 7 and 8.

This work was supported under NOAA Contracts 03-3-022-18, 03-4-022-22, NOAA Grant 04-5-158-47 and NASA Contract NAS5-23462.

APPENDIX

Background Rainfall

During GATE there were reports from aircraft scientists and ship radar scientists of significant rain from small convective clouds and stratiform clouds. For example, on 31 August rain was observed falling from cumulus with tops as low as 2.3 km (Warner, 1977). On other occasions (e.g., 18 September) heavy showers fell from congestus clouds. The echo climatology of Houze and Cheng (1977) indicates that the contribution of small, shallow convective echoes to total rainfall in and around the inner hexagon was small, perhaps a few percent. But a single estimate of "background" rainfall for the *Oceanographer* radar gave results between 5 and 20%, for instantaneous measurements over an area of about 10^5 km^2 (Martin, *et al.*, 1975).

We attribute this background rain to shallow convection, i.e., convective clouds not reaching the stature of cumulonimbi, and to stratiform cloud not originating in deep convective clouds. It is clear from comparisons with aircraft photographs (e.g., see Simpson, 1977) that these clouds can be identified in satellite picture sequences. The problem is to estimate in some simple way the amount and distribution of rain falling from such clouds.

Initially, we proposed to use cloud brightness thresholds to estimate background rainfall (Martin *et al.*, 1975). This approach failed because the thresholds appropriate for identifying small, shallow convective clouds were extremely sensitive, especially in infrared, to other clouds, such as cirrus, not connected to the rainfall. To avoid this problem we developed a scheme which is based on a satellite convective code (Martin, 1975). The satellite convective code, in turn, is an extension of the convective code proposed by Garstang and Aspliden (1974), and used by shipboard scientists during GATE.

In the original satellite convective code there were six categories, ranging from extremely depressed convection through strongly enhanced convection and post convection. The present scheme adds a seventh category of nonconvective middle-level stratus cloud. This was often observed in the GATE area, especially along the equatorial fringe of the Intertropical Convergence Zone.

The revised satellite cloud code, presented in Table A1 and Fig. A1, includes for completeness categories of deep convection (4, 5, 3D, and to some extent 3) which ordinarily would be handled explicitly by the primary scheme for convective rain estimation. The appearance of the scene for each category is described separately for visible and infrared images. Either visible or infrared

TABLE A1. A satellite convective code for estimating background rainfall.

Code/Condition	Appearance in visible	Appearance in infrared
1. Strongly depressed convection	*Predominantly* • clear (black—except in sunglint) • scattered very small to small cellular clouds (cu) • patches of cloud (sc); regular spacing, low or moderate brightness *Sometimes with* • thin, partially transparent patches and bands of layer cloud (as, ac), rapid changes in form, or • thin, veil-like layer clouds (ci), usually fast moving	*Predominantly* • clear (dark) • dark—clouds not visible • dark—may be faint cloud patches *Sometimes with* • amorphous patches and bands of cloud of moderate brightness, steady or decreasing in area, dark between clouds, rapid changes in form • amorphous patches and bands of cloud of moderate brightness, usually fast moving
2. Slightly to moderately depressed convection	*Predominantly* • many small cellular clouds (cu), often in lines and bands • bright cloud patches (sc and embedded cu), often in bands, sometimes almost solid canopy *Sometimes with* • thin, partially transparent patches and bands of layer cloud (as, ac), or • thin, veil-like or fibrous layer clouds (ci), usually fast moving	*Predominantly* • dark, small, faint clouds, seen most clearly in loop sequence with enhancement • faint but extensive cloud patches and bands *Sometimes with* • amorphous patches and bands of cloud of moderate brightness • amorphous patches and bands of cloud of moderate brightness, usually fast moving
3. Slightly enhanced convection	*Predominantly* • small to middle sized bright cellular clouds (cu and cg), often in lines or small bands *Sometimes with* • chaotic patches and masses of layer cloud (st, sc, as, ac), of moderate to occasionally high brightness, usually fading; cells penetrating • veil-like layer clouds and plumes (ci), usually fast moving, not connected with cells below	*Predominantly* • cellular or cobbled clouds of moderate brightness, in clumps, lines, or small bands *Sometimes with* • amorphous patches and masses of cloud of lower brightness, usually fading; cells penetrating • amorphous patches and plumes of cloud of moderate brightness, usually fast moving
4. Moderately enhanced convection	*Predominantly* • medium to large bright cells (cb), isolated or in broken clumps, lines, or bands; plumes of cirrus; turrets in high resolution data; expansion *Sometimes with* • chaotic patches and masses of layer cloud (st, sc, as, ac) of lower brightness	*Predominantly* • medium to large bright cells, isolated or in broken clumps, lines, or bands; expansion *Sometimes with* • amorphous patches and masses of cloud of lower brightness
5. Intense convection	*Predominantly* • solid, large masses or bands of very bright cloud, turrets in high resolution data; rapid expansion	*Predominantly* • solid, large masses or bands of very bright cloud; very rapid expansion
6. Post-convection	*Predominantly* • large flat mass or masses of bright layer cloud (cs, from old cb's), fading and becoming . . . • extensive mixture of mostly layer clouds (st, as, ac, ci, cs); formless, indistinct, sometimes chaotic, often broken; mostly moderate to high brightness; fading; in late stages may be ringed by arc clouds	*Predominantly* • large flat mass or masses of bright layer cloud, fading, and becoming . . . • extensive mixture of amorphous layer clouds, multi-leveled (usually including some bright cirrus from cb's), moderate to high brightness; fading
7. Layer cloud	*Predominantly* • extensive flat layer cloud (as), uniform high brightness, some breaks	*Predominantly* • extensive flat layer cloud, uniform moderate brightness, some breaks

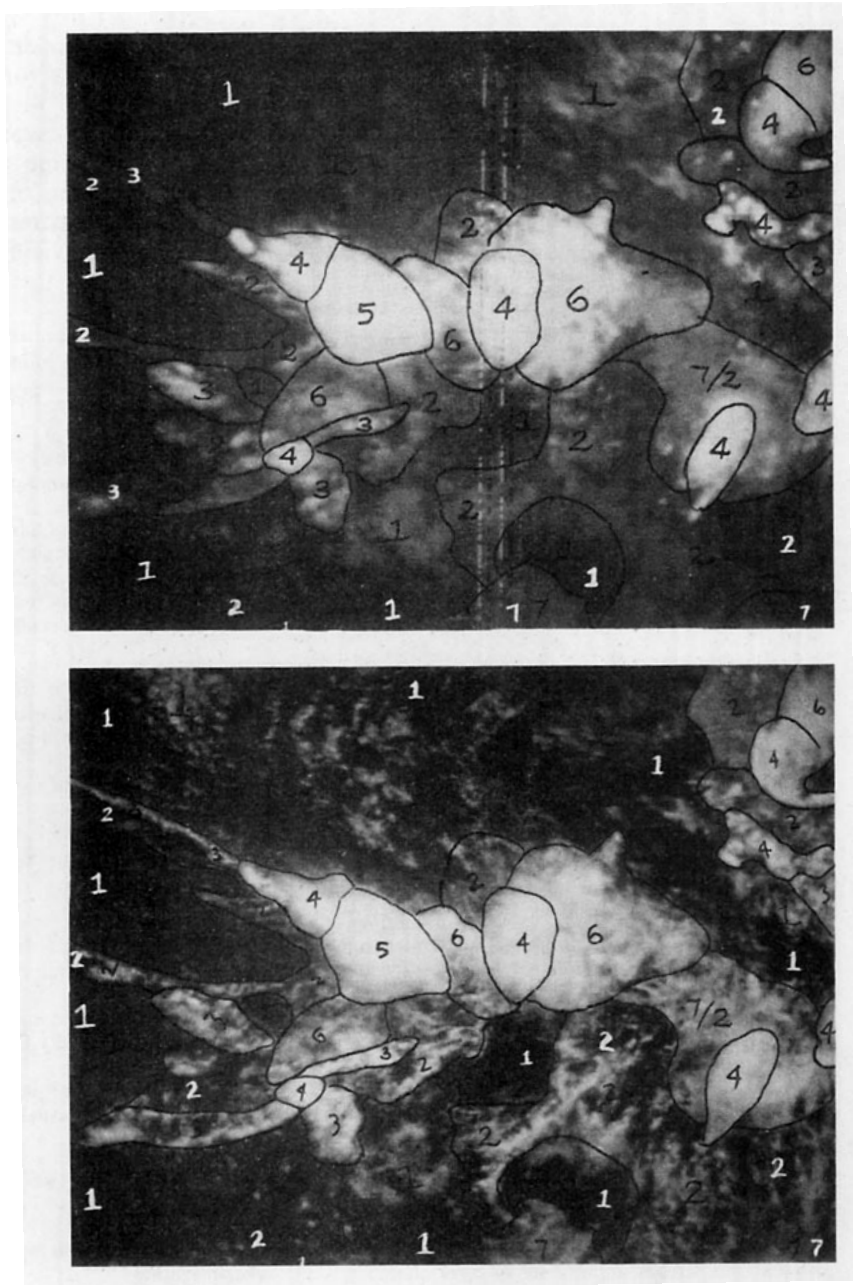

FIG. A1. Infrared (top) and visible (bottom) SMS image pair annotated with cloud type.

images could be used to determine cloud category; however, results are best if visible and infrared are used together.

To find out what rainfall rates are associated with these categories, clouds at the locations of GATE ships reporting one hourly rainfalls were assigned to one of the seven categories. In most cases three 30 min visible and infrared satellite picture pairs were used to make the assignment. Intervals of rapid change in cloud type were not included. Observed hourly rainfall rates were then tabulated for each cloud category, and plotted as frequency distributions. A similar procedure was followed for the C-array triangle, an area of 4075 km² defined by the ships *Meteor*, *Planet* and *Dallas*, for which *Quadra* radar measurements of rainfall rate have been provided by Geoff Austin of McGill University. Using the gage-radar comparisons made by Woodley *et al.* (1975) over South Florida as a guide, each of the C-array measurements was conservatively weighted to equal 10 gage measurements.

When gage and radar results are so combined (Fig. A2), we find that there is a systematic

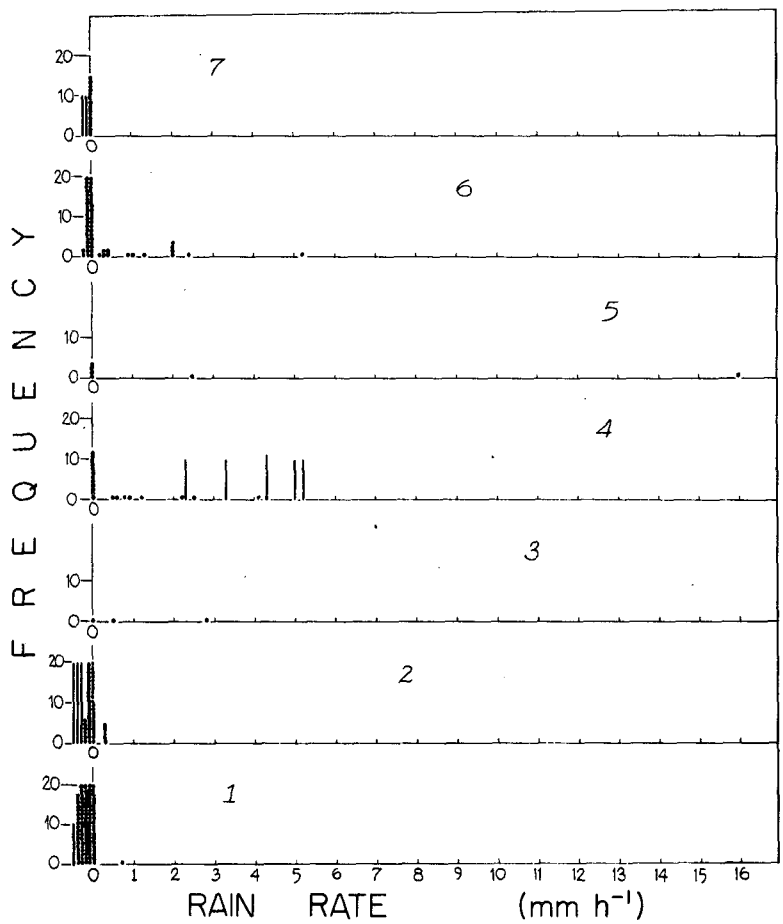

FIG. A2. Frequency distributions of rain rate, for each of the seven cloud types. Dots represent gage measurements, bars represent radar measurements. Zero rainfalls above 20 occurrences have been plotted to the left of zero frequency.

change in rainfall rate by category. The background (non-deep convective categories) 1, 2 and 7 produce practically no rainfall. Category 3, which is transitional to deep convection, apparently produces significant rain, but occurs so infrequently that for most applications it can be ignored. While the deep convective categories 4 and 5 do produce significant rainfall, these are accounted for explicitly by the area method; so too with the decaying category 6. The overwhelming bulk of rainfall in the tropical east Atlantic comes from cumulonimbus clouds. Where these are small and scattered, background rainfall may contribute a large fraction to total rainfall, but where estimates include numbers of cumulonimbus clouds, background rainfall can be ignored.

REFERENCES

Bauer, B., and J. Lienesch, 1975: VISSR data calibration. Central processing and analysis of geostationary satellite data. NOAA Tech. Memo., National Environmental Satellite Service, NOAA, Washington, DC, 64–65. [NTIS COM-75-10853/0GI].

Chatters, G. C., and V. E. Suomi, 1975: The applications of McIDAS. *IEEE Trans. Geosci. Electron.*, **GE-13,** 137–146.

Cunning, J. B., and R. I. Sax, 1977: A *Z-R* relationship for the GATE B-scale array. *Mon. Wea. Rev.*, **105,** 1330–1336.

Garstang, M., and C. I. Aspliden, 1974. Convective cloud code. University of Virginia, 22 pp.

Griffith, C. G., W. L. Woodley, J. Griffin and S. Stromatte, 1979: Satellite derived rain estimates for GATE. To be published, NOAA, Washington, DC.

——, ——, P. G. Grube, D. W. Martin, J. Stout and D. N. Sikdar, 1978: Rain estimation from geosynchronous satellite imagery—Visible and infrared studies. *Mon. Wea. Rev.*, **106,** 1153–1171.

——, ——, S. Browner, J. Teijeiro, M. Maier, D. W. Martin, J. Stout and D. N. Sikdar, 1976: Rainfall estimation from geosynchronous satellite imagery during daylight hours. NOAA Tech. Rep. ERL 356-WMPO 7, 106 pp. [NTIS PB-254 652/1GI].

Houghton, D. D., 1974: The Central Programme for the GARP Atlantic Tropical Experiment. GATE Rep. No. 3, ICSU-WMO, Geneva, 35 pp.

Houze, R. A., Jr., and C. P. Cheng, 1977: Radar characteristics of tropical convection observed during GATE: Mean properties and trends over the summer season. *Mon. Wea. Rev.*, **105,** 964–980.

Hudlow, Michael D., and R. E. Arkell, 1978: Effect of temporal and spatial sampling errors and Z-R variability on accuracy of GATE radar rainfall estimates. *Preprints 18th Conf. Radar Meteorology*, Atlanta, Amer. Meteor. Soc., 342–349.

——, and V. L. Patterson, 1979: *Gate Radar Rainfall Atlas*. NOAA Special Report (to be published).

Kilonsky, B. J., and C. S. Ramage, 1976: A technique for estimating tropical open-ocean rainfall from satellite observations. *J. Appl. Meteor.*, **15**, 972–975.

Lienesch, J. H., 1974: VISSR Thermal channel sensitivity during eclipse. Memorandum for the Record, 31 December NESS. NOAA, Washington, DC, 3 pp.

Martin, D. W., 1975: A satellite convective code. GATE Rep. No. 14, Vol. 1, WMO, Geneva, 176–181.

——, and V. E. Suomi, 1972: A satellite study of cloud clusters over the tropical North Atlantic Ocean. *Bull. Amer. Meteor. Soc.*, **53**, 135–156.

——, and W. D. Scherer, 1973: Review of satellite rainfall estimation methods. *Bull. Amer. Meteor. Soc.*, **54**, 661–674.

——, J. Stout and D. N. Sikdar, 1975: GATE area rainfall estimation from satellite images. Report on NOAA Grant 04-5-158-47, Space Science and Engineering Center, University of Wisconsin, Madison, 28 pp.

Marwitz, J. D., 1972: Precipitation efficiency of thunderstorms on the high plains. *Preprints Third Conf. Weather Modification*, Rapid City, Amer. Meteor. Soc., 245–247.

Meyer, S. L., 1975: *Data Analysis for Scientists and Engineers*. Wiley, 30–31.

Mosher, F. R., Appendix to Martin, Stout and Sikdar, 1975.

Riehl, H., and J. S. Malkus, 1958: On the heat balance in the equatorial trough zone. *Geophysica*, **6**, 503–538.

Scofield, R. A., and V. J. Oliver, 1977: A scheme for estimating convective rainfall from satellite imagery, NOAA Tech. Memo. NESS No. 86, 47 pp [NTIS PB-270 762/8Gl].

Sikdar, N. N., 1972: ATS-3 observed cloud brightness field related to a meso-to-subsynoptic scale rainfall pattern. *Tellus*, **24**, 400–413.

Simpson, J., 1977: Clouds and convection in the GATE. Report of the U.S. GATE Central Program Workshop, 25 July–12 August, NCAR, 277–287.

Smith, E. A., 1977: See Report of the U.S. GATE Central Program Workshop, 25 July–12 August NCAR, p. 189.

——, and D. R. Phillips, 1972: Automated cloud tracking using precisely aligned digital ATS pictures. *IEEE Trans. Comput.*, **C-21**, 715–729.

——, and T. H. Vonder Haar, 1976: Hourly Synchronous Meteorological Satellite-1 (SMS-1) data collected during the GARP Atlantic Tropical Experiment (GATE). [Available from World Data Center-A Data Catalog, The National Climatic Center, Federal Building, Asheville, NC 28801.]

Warner, C., 1977: Case study of GATE day 261. Report of the U.S. GATE Central Program Workshop, 25 July–12 August, NCAR, 343–355.

Wilheit, T. T., A. T. C. Chang, M. S. V. Rao, E. B. Rodgers and J. S. Theon, 1977: A satellite technique for quantitatively mapping rainfall rate over the oceans. *J. Appl. Meteor.*, **16**, 551–560.

Woodley, W. L., and B. Sancho, 1971: A first step toward rainfall estimation from satellite cloud photographs. *Weather*, **26**, 279–289.

——, —— and J. Norwood, 1971: Some precipitation aspects of Florida showers and thunderstorms. *Weatherwise*, **24**, 106–119.

——, A. R. Olsen, A. Herndon and V. Wiggert, 1975: Comparison of gage and radar methods of convective rain measurement, *J. Appl. Meteor.*, **14**, 909–928.